Journal of Power Sources 228 (2013) 47–56

Contents lists available at SciVerse ScienceDirect

Journal of Power Sources

journal homepage: www.elsevier.com/locate/jpowsour

Cathode reaction mechanism of non-aqueous Li–O_2 batteries with highly oxygen radical stable electrolyte solvent

Fuminori Mizuno [a,b,*], Kensuke Takechi [c], Shougo Higashi [c], Tohru Shiga [c], Taishi Shiotsuki [d], Nobuaki Takazawa [d], Yasunori Sakurabayashi [d], Sanae Okazaki [a], Iwao Nitta [a], Tomoki Kodama [a], Hirofumi Nakamoto [a], Hidetaka Nishikoori [a], Shinji Nakanishi [a], Yukinari Kotani [a], Hideki Iba [a]

[a] Toyota Motor Corporation, Battery Research Division, 1200 Mishuku, Susono, Shizuoka 410-1193, Japan
[b] Toyota Research Institute of North America, Materials Research Department, 1555 Woodridge Ave., Ann Arbor, MI 48105, USA
[c] Toyota Central R&D Labs., Inc., Advanced Battery Lab., 41-1 Nagakute, Aichi 480-1192, Japan
[d] Toyota Motor Corporation, Advanced Material Engineering Division, 1200 Mishuku, Susono, Shizuoka 410-1193, Japan

HIGHLIGHTS

- Oxygen radical stable electrolyte solvent is a key for rechargeable Li–air battery.
- No electrolyte decomposition was confirmed with no CO_2 gas generation.
- Discharged product was identified as Li_2O_2 by carefully analyzing objectives.
- Minor by-product (Li_2CO_3) was slightly observed on a cathode surface near O_2 gas.
- Understanding of cathode reaction contributed the improvement of cell performance.

ARTICLE INFO

Article history:
Received 9 August 2012
Received in revised form
10 November 2012
Accepted 21 November 2012
Available online 28 November 2012

Keywords:
Li–air battery
O_2 radical
Radical stability
Electrolyte solvent
Discharge product
Cathode reaction mechanism

ABSTRACT

High oxygen radical stability of electrolyte solvent is a key parameter necessary to overcome a large voltage gap in discharge–charge profiles of the non-aqueous Li–air battery. We have proposed *N*-methyl-*N*-propylpiperidinium bis(trifluoromethansulfonyl)amide (PP13TFSA) as an appropriate candidate of the electrolyte solvent. PP13TFSA based Li–O_2 cells enabled us to draw low charging voltage of around 3.3 V, lowering the voltage gap by nearly half in comparison with those of conventional carbonate-based cells (c.a. 1.4 V). Here, through the detailed analyses of discharge products, we verified the fact that the voltage gap was notably decreased by using the highly radical stable electrolyte solvent. TEM-EELS and FT-IR analyses indicated that Li_2O_2 was deposited as a discharge product. ^{13}C NMR spectroscopy suggested that no decomposed species derived from electrolyte decomposition was observed from a discharged cathode. GC–MS analyses also revealed that CO and CO_2 gases as indices of the decomposed species were not monitored at all. Above-described data substantiated a desirable discharge reaction, resulting in low charging voltage as well as small voltage gap. Design of electrolyte solvents based on their oxygen radical stability and full understanding of the cathode reaction mechanism contributed greatly to a dramatic improvement of the Li–air battery performances.

1. Introduction

Various types of vehicles have been continuously developed with new requirements and new technology. Gasoline engine as a power source has been improved again and again to enhance the driving performances, ride quality and fuel efficiency of the vehicles. Nowadays, in order to provide further high values as well as reducing some environmental burdens, hybrid vehicles equipped with both gasoline engine and rechargeable battery become mainstream. Eco-friendly vehicles consisting of rechargeable battery and renewable energy, which are typed in pure electric vehicles and fuel cell vehicles, have also received considerable attention. In any cases, the rechargeable battery is indispensable for creating their valuable vehicles and the characters of vehicles will greatly depend on the battery

* Corresponding author. Toyota Research Institute of North America, Materials Research Department, 1555 Woodridge Ave., Ann Arbor, MI 48105, USA. Tel.: +1 734 995 0172; fax: +1 734 995 2549.
E-mail address: fuminori.mizuno@tema.toyota.com (F. Mizuno).

0378-7753/$ – see front matter © 2012 Elsevier B.V. All rights reserved.
http://dx.doi.org/10.1016/j.jpowsour.2012.11.077

performances. Although lead batteries and Ni-MH batteries have been conventionally used for vehicle applications, high-performance lithium ion batteries are highly promising as an alternative power source because of their high volumetric and gravimetric energy densities. At present, novel plug-in hybrid vehicles in which a lithium ion secondary battery is installed accomplish longer cruising range and higher fuel efficiency than conventional hybrid vehicles. However, in a practical use of the lithium ion batteries, it is still impossible to drive hundreds of kilometers corresponding to a full gasoline tank, even if the state-of-art batteries are adopted. Dramatic improvement of energy density is urgently needed to achieve further increase of the cruising range, and essential is a new battery chemistry beyond the well-developed theory of lithium ion batteries.

An approach is to realize a higher energy density type Li–air battery with both technologies of Li ion battery and fuel cell. Recently, the Li–air battery has gained more and more attention because of its great potential of extremely high energy density [1–4]. This is attributed to the concept that oxygen gas is continuously supplied as a cathode fuel, utilizing lithium metal anode with high theoretical capacity. However, in practical sense, it has been very difficult to work as rechargeable Li–air batteries because of well-known dendrite formation of Li metal anode and its high reactivity with air [5,6]. The other major challenge that lies for rechargeability and cycleability is an insulative product formed on a cathode. Although the insulative product is a by-product of a huge energy source, a difficulty in decomposing the product prevents us from constructing the rechargeable Li–air battery system instantaneously. Since Abraham's group first reported that a prototype Li–air battery which consisted of non-aqueous gel electrolyte and catalyzed cathode was successfully discharged and recharged [1], many efforts have been devoted to establish the Li–air battery as a rechargeable system. Read et al. and Kuboki et al. focused on the carbon materials and electrolyte solvents to improve the battery performances [2,3]. In addition, Bruce's group first discussed the cycleability for long operation in the commonly used carbonate electrolyte system [4]. Owing to their great achievements, the potential and issues of the Li–air battery have been extensively understood in terms of material chemistry, electrochemistry and computational study [7–25].

One of the biggest issues is a large voltage hysteresis between discharging and charging cycles [4,15]. In the carbonate-based electrolyte systems, it was observed that the discharge and charge voltages were 2.6 V and 4.0 V, respectively, and therefore, a large voltage gap of 1.4 V was produced, resulting in lowering of energy efficiency of the Li–air battery. At present, through the analyses of cathode reaction products, the reason why the hysteresis was obtained in the conventional electrolyte systems has been clarified. It was confirmed that not Li_2O_2 but carbonate species (XCOOLi, X = alkyl group or Li) were deposited on a discharged cathode, and furthermore, not O_2 gas but CO_2 gas evolved during recharging [12,15,16,18–20]. The carbonate species were considered to be the by-products caused by decomposition of carbonate-based electrolytes due to O_2 radical species (O_2^-, LiO_2) as discharge reaction intermediates, and CO_2 gas evolved as a consequence of the decomposition of carbonate species. Thus, it can be stated that the main reason for the large voltage gap was derived from two different cathode reactions during discharging and charging as follows;

Here, we focused on the evolution of oxygen radical species in the non-aqueous media. It is well known that the oxygen anion radical inherent in strong nucleophillicity naturally attacks the molecules and ions with a positive charge. A main target to be attacked by O_2 radical species was the carbonate solvent whose constituent carbon was locally and positively charged [23]. As a result, a ring opening of the carbonate solvent occurred, forming the decomposed species on a cathode [12,16]. We have taken three countermeasures to this unwanted cathode side reaction. First is not to produce the oxygen anion radical via one electron reduction process, that is, to realize direct four electron reduction of oxygen in an aprotic media ($O_2 + 4e^- \rightarrow 2O^{2-}$, $2O^{2-} + 4Li^+ \rightarrow 2Li_2O$). Second is to promote a subsequent reaction of the radical species intermediates with lithium ion ($LiO_2 + e^- + Li^+ \rightarrow Li_2O_2$). Last is to let the radical species stabilize in an aprotic media. The first countermeasure will be achieved by an oxygen reduction catalyst, but the desirable catalyst is not reported in the literature yet according to the author's knowledge. The second approach was carried out in the concentrated electrolyte solution in which the concentration of supporting lithium salt was higher than 1 M. In cyclic voltammograms, an anodic oxidation at higher potential which is observed as a trace of the side reaction was hampered to some extent, and furthermore, both cathodic and anodic currents corresponding to O_2 reduction and Li_2O_x decomposition were successfully increased. However, a large voltage gap of 1.4 V still appeared in the discharge–charge profiles, and as a consequence, it was impossible to shut off the side reaction completely. Then, we have focused on the stabilization of the radical species themselves, that is, enhancing the tolerance of electrolyte solvent against the oxygen radicals. Solvent screening was performed using electrochemical technique combined with first principles calculations [23] and non-electrochemical technique with KO_2 chemical [24]. Based on the results, we have proposed *N*-methyl-*N*-propylpiperidinium bis(trifluoromethansulfonyl)amide (PP13-TFSA) ionic liquid as an appropriate candidate of electrolyte solvent for Li–air battery. Because of its comparably charge neutrality (less local positive charge), the O_2 anion radical stably existed in the electrolyte solution, resulting in the nice reversibility of O_2 redox reaction in the cyclic voltammogram [23]. Also, the ionic liquid was much stable against a superoxide, KO_2 similar to LiO_2 as an intermediate [24]. Moreover, the ionic liquid is applicable to an open system as expressed in the Li–air battery because of its hydrophobicity and nonvolatility in nature. It has been, thus, believed that the PP13TFSA ionic liquid can be used to construct the viable Li–air rechargeable battery. Finally, we have presented that the PP13TFSA based Li–O_2 cells exhibited much lower charging voltage of around 3.2 V and lower voltage gap of about 0.75 V than the carbonate-based ones [23]. The improvements of voltage hysteresis and energy efficiency of the battery were achieved by stabilizing the oxygen radical species in the PP13TFSA based system. It is, therefore, suggested that the low charging voltage and smaller voltage gap will be attributed to the following cathode reaction, which is not a completely reversible reaction but is composed of the same final products of Li_2O_2 and O_2.

Discharge @ 2.6 V : $O_2 + e^- \rightarrow O_2^-$ (oxygen anion radical, herein called oxygen radical species)

$Li^+ + O_2 + e^- \rightarrow LiO_2$ (oxygen radical derivative, herein called oxygen radical species)

Oxygen radical species + carbonate solvent + Li + $\rightarrow$ XCOOLi (X = alkyl group, Li)

Charge @ 4.0 V : XCOOLi $\rightarrow Li^+ + CO_2 + e^-$ + X derivatives($XO^{\cdot}$)

Discharge @ 2.5 V : $O_2 + e^- \rightarrow O_2^-$ (Oxygen reduction)

$Li^+ + O_2 + e^- \rightarrow LiO_2$ (Formation of intermediate)

$2LiO_2 \rightarrow Li_2O_2 + O_2$ (Disproportionation)

Charge @ 3.25 V : $Li_2O_2 \rightarrow 2Li^+ + O_2 + 2e^-$ (Direct decomposition)

It has been already reported that O_2 gas evolved when Li_2O_2, a desired discharge product, was decomposed by electrochemically charging [4,18]. Therefore, the existence of Li_2O_2 after discharging will be a very important evidence to satisfy the above expectation in our selected system.

In this paper, we demonstrated the discharge–charge behaviors of the PP13TFSA based Li–O_2 battery under several operating conditions, and then we identified the final products obtained on the discharged cathode by using lots of analytical techniques. Unlike in the case of the carbonate system, we verified that the above-described desired cathode reaction processes occurred. The detailed cathode reaction mechanism during discharging will be discussed in term of the oxygen radical stability of electrolyte solvent and will be summarized in a cathode reaction route map. Finally, based on our analytical results, some remaining future issues will be addressed.

2. Experimental

2.1. Electrochemical tests

Non-aqueous Li–O_2 batteries were constructed as described in the previous papers [15,23,24]. Air cathode was composed of Ketjen Black (Ketjen Black International, ECP600JD), MnO_2 catalyst (Mitsui Metal Mine, EMD) and PTFE binder (Daikin, battery grade) with a weight ratio of 90:0:10 or 80:10:10. This mixture was pelletized by using roll pressing, and then the pellet sheet was dried at 120 °C overnight under vacuum. Battery grade *N*-methyl-*N*-propylpiperidinium bis(trifluoromethansulfonyl)amide (PP13TFSA, Kanto Chemical) or typical organic solvents (Kishida Chemical) such as propylene carbonate (PC), a mixture of ethylene carbonate (EC) and diethylcarbonate (DEC), γ-butyrolactone (GBL) and tetraethyleneglycol dimethylether (TEGDME) were used as an electrolyte solvent. Lithium bis(trifluoromethansulfonyl)amide (LiTFSA, Kishida Chemical, battery grade) was mixed into the solvent so as to be the salt concentration of 0.32 mol kg^{-1} and 1.0 mol l^{-1} in the PP13TFSA and PC solutions, respectively. The water amounts of both electrolytes were checked by Karl-Fischer technique, keeping less than 50 ppm. Substantially thick lithium metal (Honjo Metal, battery grade) was used as an anode and the current collectors of anode and cathode were the stainless steel disk and mesh, respectively. These components were set into our custom-made cell equipped with a gas cylinder under Ar atmosphere, and then the inert gas was completely replaced with high purity O_2 gas at ambient temperature. The assembled Li–O_2 cells were tested at various conditions in a charge-discharge machine (Nagano, BTS2004H). Current densities were constantly set in the region from 0.01 to 0.40 mA cm^{-2} and cut-off voltages were 2.0 V and 3.85 (or 4.5) V in discharge and charge, respectively. Also, the operating temperatures were 25 °C and 60 °C. Before testing, the cells were kept for 3 h at an operating temperature in order to fully dissolve oxygen gas into the electrolyte solutions.

2.2. Characterization of discharged cathode

In order to identify the final reaction products after discharging, discharged cathodes were rinsed with anhydrous non-aqueous solvents and then were dried in an Ar glove box at room temperature. Color of the discharged cathode turned to gray or white from original black because of discharge precipitates.

Cathode surface and its cross section before and after battery testing were observed in a field emission scanning electron microscope (FE-SEM) instrument (Hitachi High-Tech., S4800). High magnification images of discharge products as well as non-discharged and discharged cathodes were recorded on a field emission transmission electron microscope (FE-TEM) instrument (Hitachi High-Tech., HF2000). Some pieces of discharge products were sampled from a discharged cathode side exposed to O_2 atmosphere and then were carefully set on a well-dried Cu grid under an Ar glove box. Cross section samples were also prepared from the same cathode side by a focus ion beam (FIB) technique on a machine (Hitachi High-Tech., FB2100) equipped with a Ga ion gun. The cathodes for cross section TEM observation were scraped until the thickness of thin film was around 200 nm. All samples were transferred into both instruments with no exposure to air using an original transfer vessel, and then their morphologies were carefully checked under the optimized conditions so as not to give heavy sample damages due to electron beam. Also, electron energy-loss spectroscopy (EELS) and electron diffraction (ED) were performed on another FE-TEM instrument (FEI, TECNAI G^2) to distinguish the chemical composition of Li compound. EELS spectra of standard materials, Li_2O_2, Li_2O, Li_2CO_3, LiOH, LiF and CH_3COOLi, were collected in advance, and then were compared with the spectrum of the discharge product. To analyze the difference of those spectra precisely, the spectrum of background was removed from each raw spectrum, and then each raw spectrum was differentiated twice. Furthermore, to judge roughly whether desirable discharge product was formed or not, the basicity, pH of an aqueous solution in which the discharged cathode was dissolved was measured by a pH meter (Horiba, D-51). The aqueous solutions were obtained by fully immersing discharged cathodes in the distilled water of 50 ml.

Finally, in order to check the existence of by-products due to a side reaction, nuclear magnetic resonance (NMR) spectroscopy, Fourier transform infrared (FT-IR) spectroscopy, and furthermore, gas chromatograph/mass spectroscopy (GC–MS) were carried out. Carbonate species were used as an index of the by-products. To obtain the total information of the discharged cathode, ^{13}C NMR spectra were recorded on an apparatus (Agilent, INOVA) with a magnetic frequency of 75.399 MHz. The discharged cathode was fully immersed in the D_2O solvent under a dew point of −40 °C and then the supernatant solution was poured in a quartz tube. FT-IR spectra were also obtained on a spectrometer (Magna550, ThermoFischer Sci.) with a photoacoustic equipment, which enables us to obtain the depth information to some extent in spite of strong absorption of black-colored samples. Samples were set on a special holder under a dew point of −40 °C and high purity He gas was always purged during the measurement. Furthermore, the gas generated during recharging process was stored in our original gas tank, and then was analyzed on a GC–MS apparatus (Shimazu, QD5500). Since the sample gas was stored with original O_2 gas during discharging and recharging to avoid gas contamination from outside of the battery, CO and CO_2 gases as indices of side reaction were mainly monitored.

3. Results and discussion

3.1. Li–O_2 battery performances

First, the discharge–charge behaviors in the Li–O_2 batteries with PP13TFSA as an electrolyte solvent were compared with those of the typical carbonate-based batteries. Fig. 1 shows the initial discharge and charge curves of the (a) PP13TFSA based and (b) carbonate-based Li–O_2 cells at 25 °C. Applied current densities for discharging and charging were 0.02 and 0.01 mA cm^{-2}, respectively. Discharge–charge capacities were normalized by the total weight of cathode. In the PP13TFSA based system (a), a flat discharge plateau was observed at around 2.5 V and a discharge capacity reached around 2000 mAh g^{-1}. After recharging, a charge plateau was obtained in the region from 3.0 V to 3.4 V, and then the initial charge capacity was around 1800 mAh g^{-1}. On the other hand, the voltage profile in the carbonate-based system (b) was considerably different from that of the system (a), although the difference of capacity was observed. Carbonate-based Li–O_2 cell was discharged at around 2.7 V and then was recharged over 4.1 V as reported so far [4,15]. As a result, the voltage gap between discharging and charging profiles was over 1.4 V. This gap was caused by the electrolyte decomposition of carbonate solvents due to O_2 radical and the subsequent decomposition of decomposed species. However, in our proposed system (a), not only low charging voltage of around 3.3 V but also small voltage gap of about 0.75 V was successfully achieved. The charging voltage was comparably close to the theoretical potential (2.96 V) of Li_2O_2 to be decomposed directly via 2 electron transfer process, indicating that Li_2O_2 must be formed as a main discharge product. Detailed investigation of the discharge product will be described later. As reported in our publication [23], highly oxygen radical stable electrolyte solvent should bring about the enhancement of the discharge–charge properties of the Li–O_2 batteries. It can be, therefore, stated that finding a suitable electrolyte for a Li–air battery is an important key to improve the Li–O_2 battery performances. As in Fig. 1, the nice battery performance was shown in spite of high viscous electrolyte solvent (PP13TFSA) at 25 °C. According to our previous paper [23], one tenth of the discharge capacity drawn in Fig. 1 was observed at 60 °C. This dramatic improvement was supported by rearranging cell configuration. Our previous custom-made cell had a big distance between anode and cathode, 5 mm to avoid unwanted short circuit due to dendrite growth from Li anode and to shut off the influences of electrolyte evaporation, air contaminants and so on. However, to further improve the discharge–charge properties of the PP13TFSA based Li–O_2 cell, the reconstructed cell where a commonly used separator was installed between anode and cathode was strongly needed. Since PP13TFSA is a nonvolatile liquid and is fortunately an electrolyte solvent enabling us to suppress the Li dendrite growth to some extent [26], the cell performances were hopefully improved with the new cell configuration.

Fig. 2 shows the discharge curves of the PP13TFSA based Li–O_2 batteries at various operating conditions. Line (a) denotes the data obtained when the current density of 0.10 mA cm^{-2} was applied at 25 °C. Lines (b), (c) and (d) denote the data of 0.10, 0.20 and 0.40 mA cm^{-2} operated at 60 °C. Inset figure shows the discharge capacities as a function of applied current densities. Open and closed circles denote the operation temperatures at 25 °C and 60 °C, respectively. High discharge capacity of 2000 mAh g^{-1} was obtained under a constant current density of 0.02 mA cm^{-2} at 25 °C, while it was not maintained under 0.10 mA cm^{-2} and decreased down to around 400 mAh g^{-1}. When the operating temperature was set at 60 °C, much higher capacity of around 2900 mAh g^{-1} was achieved under 0.10 mA cm^{-2} (line (b)). The enhancement of the initial capacity must be attributed to higher mass transfer of Li^+/O_2 in both electrolyte and cathode parts at 60 °C. However, even at 60 °C, the discharge capacity was suddenly decreased with an increase in an applied current density (i.e. 2900–200 mAh g^{-1}). Although further improvement is now ongoing, the proposed Li–O_2 batteries delivered comparably nice performance at the present stage.

3.2. Identification of final products after discharging

In order to clarify whether the expected reaction really occurred by applying the PP13TFSA ionic liquid to the Li–O_2 cell, both discharged cathode and discharge products were analyzed in detail, and in the last section, the cathode reaction mechanism was summarized with that of the PC based system. To analyze the discharged cathodes with almost the same capacity, the PP13TFSA and

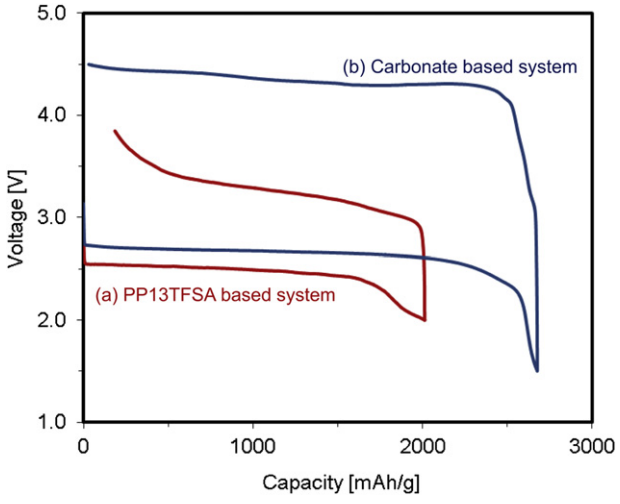

Fig. 1. Initial discharge and charge curves of the (a) PP13TFSA based and (b) typical carbonate-based Li–O_2 cells at 25 °C. Applied current densities for discharging and charging were 0.02 and 0.01 mA cm^{-2}, respectively.

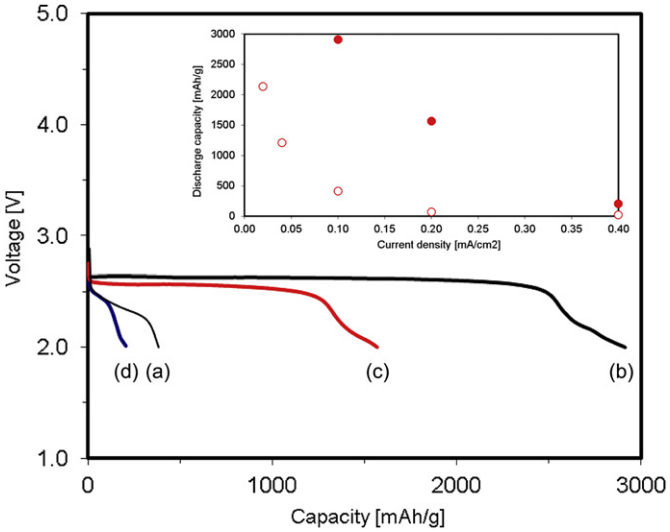

Fig. 2. Discharge curves of the PP13TFSA based Li–O_2 batteries at various operating conditions. Line (a) denotes the data obtained when the current density of 0.10 mA cm^{-2} was applied at 25 °C. Lines (b), (c) and (d) denote the data of 0.10, 0.20 and 0.40 mA cm^{-2} operated at 60 °C. Inset figure shows the discharge capacities as a function of applied current densities. Open and closed circles denote operation temperatures at 25 °C and 60 °C, respectively.

PC based cells were tested under 0.02 mA cm^{-2} at 60 °C and 25 °C, respectively.

First, the morphology of discharge products was carefully checked. Fig. 3 shows the FE-SEM images of the following cathodes; (a) before discharging, (b) after discharging in the PP13TFSA based electrolyte and (c) after discharging in the PC based electrolyte. Fresh cathode in the image (a) was composed of chain-like structures with primary particles of around 20–50 nm in diameter, which are very unique for carbon black. Furthermore, many pores with various sizes were formed between carbon black particles. After discharging, two contrasting cathode surfaces were observed. In the cathode (b) obtained by using the PP13TFSA based electrolyte, the original carbon black particles seemed to be covered by discharge products and the size of carbon particles grew homogeneously. On the other hand, the texture of original carbon black could not be observed in the cathode (c) with the PC based electrolyte, and instead, the discharge products similar to passivation film appeared on the cathode surface. High magnification images of the discharged cathodes obtained by FE-TEM observation were shown in Fig. 4. Fig. 4 shows the bright field images of (a) discharge

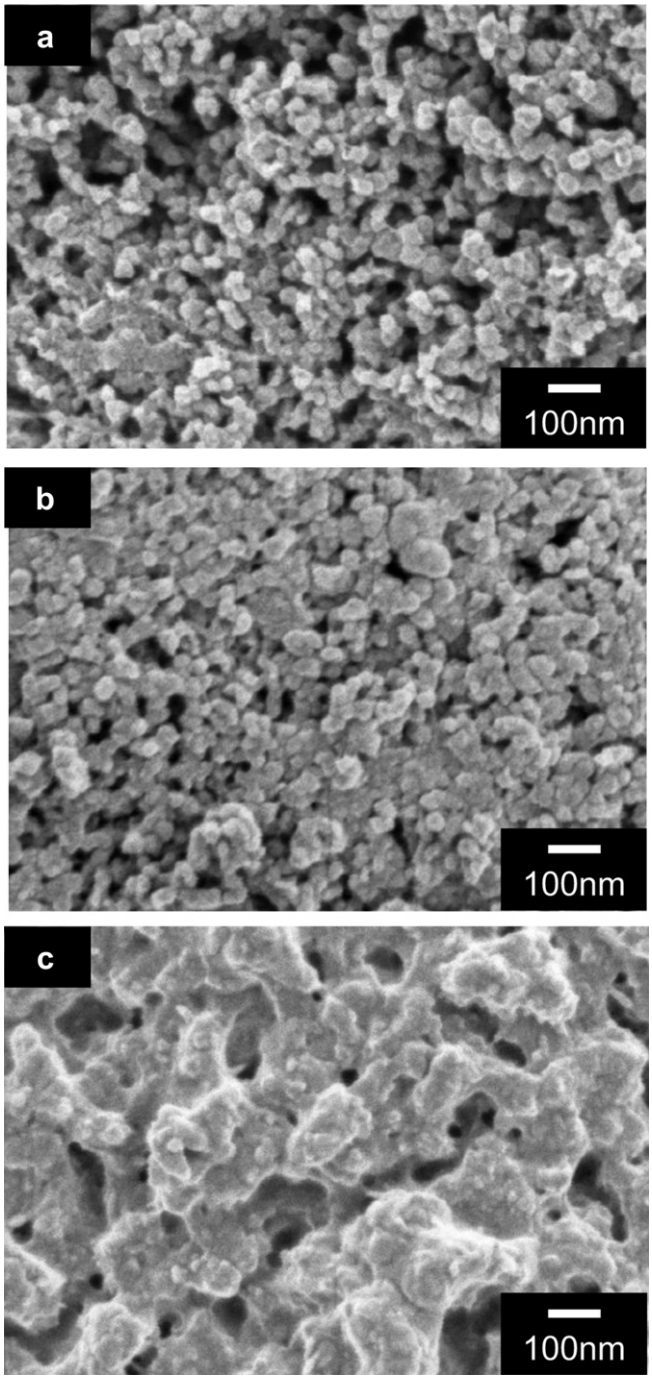

Fig. 3. FE-SEM images of (a) fresh cathode before discharging, (b) discharged cathode in the PP13TFSA based electrolyte and (c) discharged cathode in the PC based electrolyte.

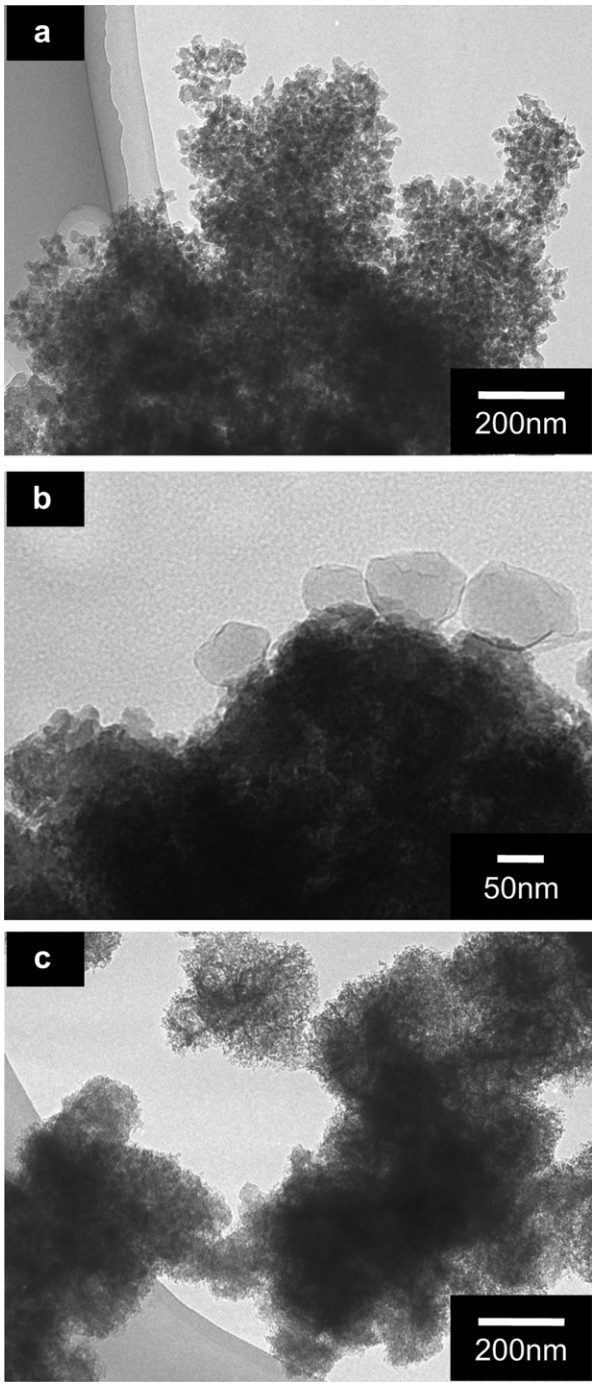

Fig. 4. Bright field images of (a) discharge products in the PP13TFSA based cell, (b) another discharge products in the PP13TFSA based cell and (c) discharge products in the PC based cell.

products obtained in the PP13TFSA based cell, (b) another discharge products in the PP13TFSA based cell and (c) discharge products in the PC based cell. In the pictures (a) and (c), many primary particles of around 20 nm in diameter were agglomerated together on carbon black particles, while in the picture (b), there existed four particles formed on a carbon coated MnO_2 catalyst, which were enlarged up to 100 nm in diameter. Moreover, the morphology of the aggregates as in the pictures (a) and (c) was very different in type of electrolyte solvents. Granular aggregates were observed on the discharged cathode of the PP13TFSA based cell, whereas mossy aggregates were obtained from that of the PC based cell. It was, thus, found that the size and texture of discharge products strongly depended on the operating battery system and the reaction site in the cathode. Further study on the morphological control of discharge products is now in progress [27–29].

Next, the chemical composition of discharge products was examined. EDX analyses indicated that oxygen signal was just obtained in the PP13TFSA based battery cathodes, while the elements of carbon and oxygen were detected in the PC based ones. Raman spectroscopy was commonly used as a tool to distinguish Li_2O_2 from Li_2O and other Li compounds. Raman bands attributed to Li_2O_2 (780 cm^{-1}) or Li_2O (520 cm^{-1}) were not observed in the cathode obtained with the PC based electrolyte, and instead, some characteristic bands including C=O bond (1080 and 710 cm^{-1}) and C–H bond (around 3000 cm^{-1}) were obtained and were assigned to lithium alkylcarbonate. On the contrary, in the cathode with the PP13TFSA based electrolyte, it was very difficult to collect the Raman signal derived from lithium compounds because of strong fluorescence of carbon black. Probably, the difference in the surface morphology of the discharged cathode as shown in Fig. 3 would notably affect the detection of Raman spectra. X-ray diffraction did not give any crystalline information enough to detect because of the low sensitivity and low crystallinity of discharge products in this experiment. Also, as reported by Freunberger et al. [16,17] and us [15], FT-IR analysis is a nice technique to detect Li compounds with Raman spectroscopy. Characteristic bands due to Li_2O_2 and Li_2CO_3 were separately observed (FT-IR spectra will be shown later in Fig. 8). Since carbon materials themselves have unique bands for some functional groups of carbonate, carbonyl and so on, the obtained spectra must be carefully assigned. On the other hand, our ^{7}Li solid state NMR spectra for the discharged cathodes indicated that the spectra of actual samples showing a broad peak at around 0 ppm were difficult to be qualitatively analyzed, because the chemical shifts of all the standard materials were concentrated close to 0 ppm. As already reported by Xiao et al. [20], those spectra will be clearly distinguished by using ultra-high-field solid state NMR technique with ^{6}Li species. Otherwise, as reported by Goward et al. [30], the spectra of actual samples will be distinguished if high resolution NMR measurements were carried out. Very recently, soft X-ray absorption fine structure (XAFS) spectroscopy for the discharged cathodes has been performed based on the K edge absorption end of Li and O elements. As recently reported by Lu et al. [21], the absorption spectra will be qualitatively analyzed with those of standard materials, although the analysis by means of sample current method is very sensitive for the surface of powder and electrode.

Finally, we reached the conclusion that TEM-EELS analyses were very useful to identify the chemical composition with observing objectives. Although we confirmed that a strong electron beam during observing caused the damage of sample, we have succeeded in collecting the EELS information with the observing views by adjusting the analyzing condition. Fig. 5(a) shows the EELS spectra of a discharge product pictured in Fig. 4(b). Top of the graph represents the modified spectra in which the background spectra were extracted from the raw spectra, while the bottom does the

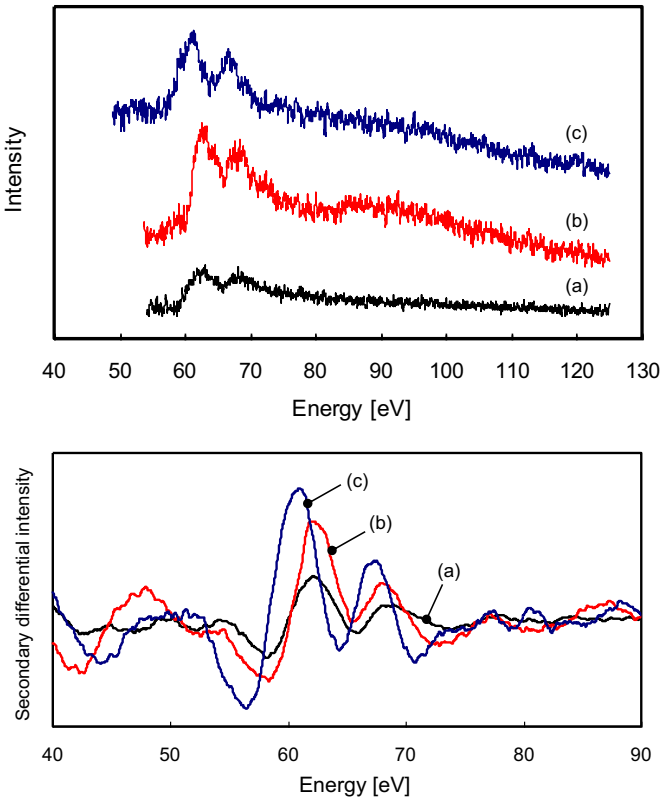

Fig. 5. EELS spectra of (a) a discharge product sample pictured in Fig. 4(b). The spectra of (b) Li_2O_2 and (c) Li_2CO_3 are shown for the comparison. Top of the graph represents the modified spectra in which the background spectra were extracted from the raw spectra, while the bottom does the results obtained by secondary differential of the raw spectra.

results obtained by secondary differential of the raw spectra. The spectra of (b) Li_2O_2 and (c) Li_2CO_3 as standard materials are shown for the comparison. It was confirmed in advance that all of the spectra were characteristic of Li compounds and were completely distinguished in terms of peak position and peak shape. As reported so far, the main product obtained in the PC based cells was carbonate species including Li_2CO_3 [15,16,18–20]. However, as can be seen, the spectrum of the discharge product obtained in the PP13TFSA based media was very close to that of Li_2O_2. Since the spectrum of the sample did not correspond to those of other Li compounds, it can be stated that the discharge product was identified as Li_2O_2 in the PP13TFSA based cells. To support this identification, pH of aqueous solutions made by immersing discharged cathodes was compared in the PP13TFSA and PC based systems. Discharged cathode in the PP13TFSA based system had a higher pH value of around 11 than that of the PC based system (~8.5), indicating that the cathode deposits obtained in the PP13TFSA based system consisted in strong basic compounds such as lithium peroxide, and this result is consistent with that of the above TEM-EELS analyses. It was, thus, found that Li_2O_2 was deposited on the discharged cathode by using the PP13TFSA based electrolyte solvent with high oxygen radical stability.

3.3. Possibility of side reaction due to electrolyte decomposition

Li_2O_2 as a main product was detected, but a side reaction related with O_2 radical species may occur on a cathode. ^{13}C NMR measurements were done to check the trace of by-products in both systems. Fig. 6 shows the ^{13}C CP-MAS NMR spectra of D_2O solutions obtained by immersing the (a) PP13TFSA and (b) PC derived

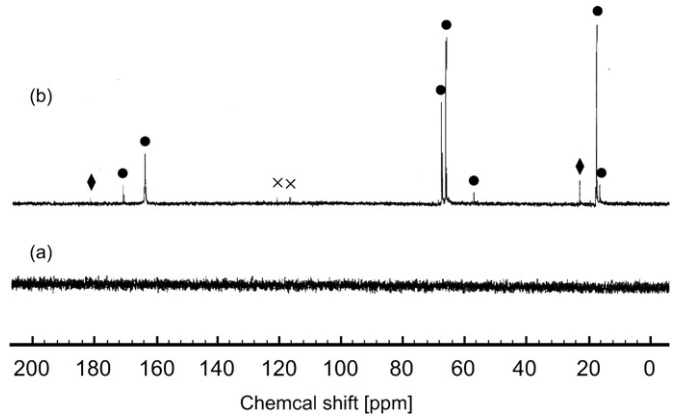

Fig. 6. ^{13}C CP-MAS NMR spectra of D_2O solutions obtained by immersing the (a) PP13TFSA and (b) PC derived discharged cathode. The symbol of circle was assigned to analogs of lithium alkylcarbonate, RO–(C═O)–OLi (R = alkyl group) including Li_2CO_3 and the diamond was to lithium acetate. The cross mark was due to TFSA anion.

discharged cathode. In the profile (b), signals derived from carbonate species were observed. The symbol of circle was assigned to analogs of lithium alkylcarbonate, RO–(C═O)–OLi (R = alkyl group) including Li_2CO_3 and the diamond was to lithium acetate. It was obvious that the PC solvent was decomposed by O_2 radical species and then the decomposed species such as lithium alkylcarbonate were precipitated on the cathode during discharging. On the other hand, no such signal was obtained in the profile (a), even if the sample concentration and number of scans for measuring were increased. Also, no spectrum change was seen even in the electrolyte before and after discharging. In addition, ^1H NMR results indicated that characteristic signals assigned to the decomposed species of the electrolyte solvent, which can be seen in the PC derived discharged cathode, were not clearly observed in the PP13TFSA derived cathode. It can be, thus, stated that the severe decomposition of electrolyte solvent as in the PC based system did not occur for the PP13TFSA based system.

From compositional viewpoint of the gas evolved after recharging, the possibility of by-products was checked. Quantitative analyses were carried out by gas chromatography for the gases stored during the initial recharge, and the gas compositions and their normalized concentration were listed in Table 1. Amounts of the evolved gases were normalized by the electrical quantity during recharging. In the organic electrolyte systems, CO and CO_2 gases, which were derived from a side reaction of electrolyte solvent with O_2 radical species during discharging, were generated from all solvents we attempted. Tetraethyleneglycol dimethylether (TEGDME) solvent brought about the lowest amounts of such gases among the organic systems. This result was supported by the previous fact that the Li_2O_2 formation was confirmed in the TEGDME based Li–O_2 cells, but Li_2CO_3 was gradually deposited with increasing cycle number [8,17]. On the other hand, in the PP13TFSA based system, CO and CO_2 gases were not generated at all, which was well linked with the results of Figs. 5 and 6. Instead, large amounts of O_2 gas corresponding to a charge capacity was confirmed when the cell was recharged under an Ar atmosphere. H_2 gas generation was also observed, most probably because of a non-electrochemical reaction of lithium metal with the PP13TFSA ionic liquid and very small amounts of original water contained inside the cells.

Table 1
Compositions and their normalized concentration of various gases stored during the initial charge by gas chromatography. Amounts of the evolved gases were normalized by the electrical quantity during charging.

Electrolyte solvent	Classification	Norm. gas conc. [L/Ah]		
		H_2	CO	CO_2
PP13TFSA	–	0.311	0.000	0.000
EC-DEC	Carbonate	0.114	0.028	0.555
PC	Carbonate	0.035	0.014	0.676
GBL	Lactone	0.579	0.079	0.826
TEGDME	Ether	0.197	0.007	0.001

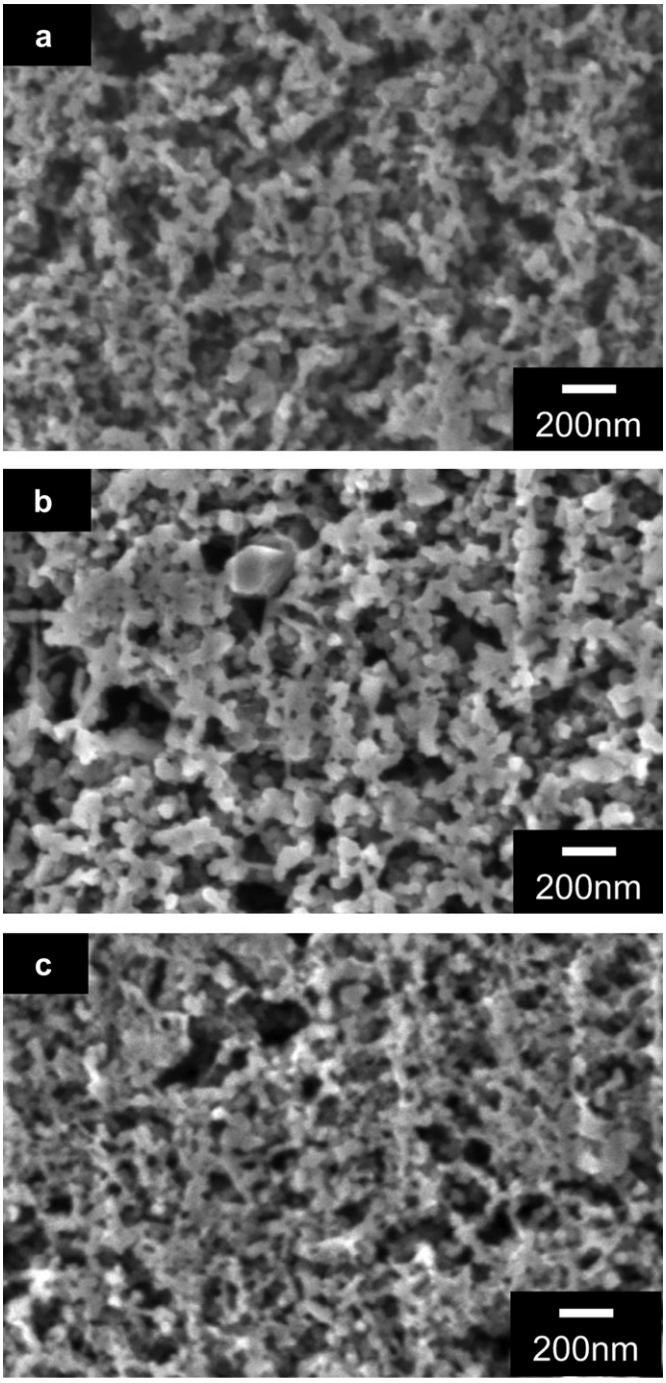

Fig. 7. Cross section images of cathodes before and after the discharge–charge measurements in the PP13TFSA based media. Image (a) denotes the cathode before testing, and the images (b) and (c) denote the ones after discharging and recharging, respectively.

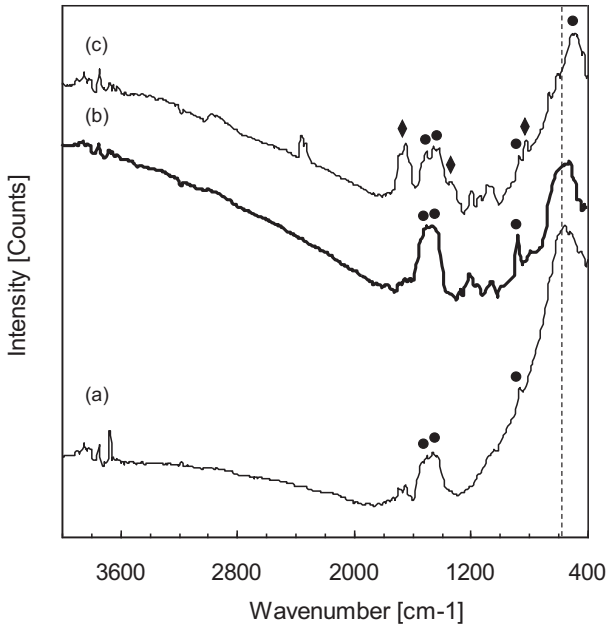

Fig. 8. FT-IR spectra of discharged cathodes by photoacoustic spectroscopy. The spectrum of fresh cathode including Li_2O_2 is shown in Fig. 8(a). The spectra (b) and (c) denote the discharged cathode obtained in the PP13TFSA and PC based cells, respectively. The dotted line denoted the peak position of Li_2O_2. The symbol of circle was assigned to Li_2CO_3, while the diamond was to lithium alkylcarbonate.

Cross section images of cathodes before and after the discharge–charge measurements in the PP13TFSA based media were described in Fig. 7. Image (a) denotes the cathode before testing, and the images (b) and (c) denote the cathodes after discharging and charging, respectively. Although particle sizes of carbon black increased after discharging, the sizes were mostly recovered after recharging. Since discharge products completely disappeared after recharging, the gas chromatogram and SEM images in the PP13TFSA based system substantiated the fact that no by-products caused by the decomposition of electrolyte solvent was generated on the discharged cathode.

However, another species, which was not due to the above-described electrolyte decomposition, was detected on a discharged cathode. Fig. 8 shows the FT-IR spectra of discharged cathodes by photoacoustic spectroscopy. The spectrum of fresh cathode including the Li_2O_2 reference material is shown in Fig. 8(a). The spectra (b) and (c) denote the discharged cathode obtained in the PP13TFSA and PC based cells, respectively. Li_2O_2 containing cathode (a) as a reference sample had a strong absorption peak of Li_2O_2 at around 530 cm^{-1} (dotted line). A broad peak of about 1500 cm^{-1} and a narrow peak of 860 cm^{-1} corresponding to Li_2CO_3 (symbol of circle) were obtained, indicating that Li_2O_2 and carbon (especially for surface functional groups) might be chemically reacted. Discharged cathode (c) in the PC based media had unique peaks, which were assigned to lithium alkylcarbonate, at around 1630 and 1310 cm^{-1} (symbol of diamond) as well as some peaks corresponding to Li_2CO_3. The detection of lithium alkylcarbonate was in good agreement with the NMR result of Fig. 6(b). On the contrary, the cathode (b) in the PP13TFSA based media possessed a peak specific to Li_2O_2 as a discharge product, which is consistent with the TEM-EELS result shown in Fig. 5. However, some bands assigned to Li_2CO_3 were also detected.

In order to make sure of the existence of Li_2CO_3 in the PP13TFSA based system, TEM observation of the discharged cathode cross section was carefully conducted. Fig. 9 shows the bright field images of the cathode cross section thin films fabricated by a FIB technique. Pictures (a) and (b) represent the cathodes before and after discharging, respectively. Fresh cathode (a) consisted in a characteristic texture of carbon black and a MnO_2 particle which is comparably dark gray in color. After discharging, there existed not only mossy texture (seen in a white dotted circle), but also very small black particles of less than 20 nm in size. The black particles were just confirmed near the cathode surface exposed to O_2 atmosphere, but it was not detected around the opposite side. Inset figure shows the selected area electron diffraction (SAED) pattern of the black particle. Obvious spots were clearly assigned to Li_2CO_3. The Li_2CO_3 particles were presumed to be deposited at the interface between Li_2O_2 and carbon black because of strong oxidation capability of Li_2O_2. Recently, the reactivity of Li_2O_2 and carbon during recharging has been discussed by McCloskey et al. in the ether based system [25]. In addition, Peng et al. have very recently reported that quite

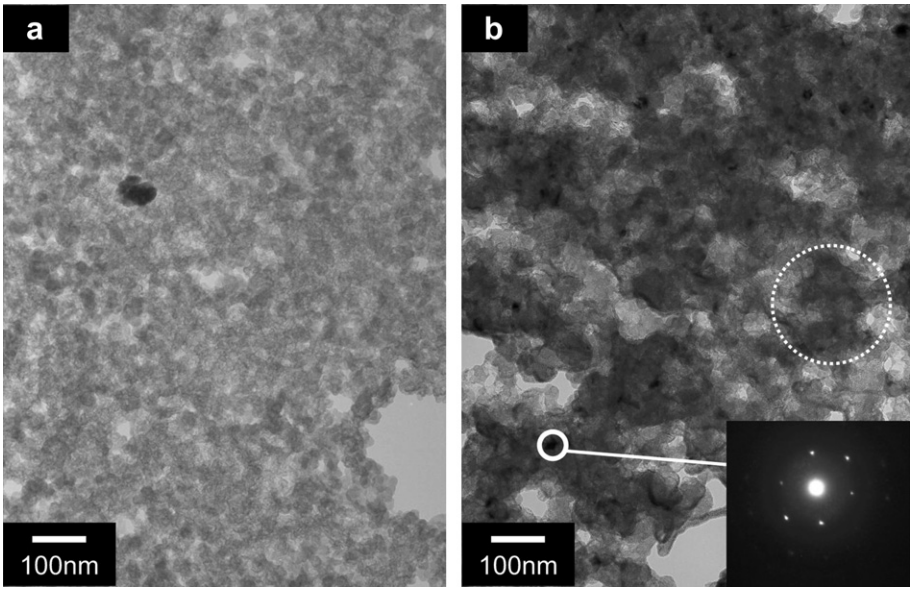

Fig. 9. Bright field images of the cathode cross section thin films fabricated by a FIB technique. Pictures (a) and (b) represent the cathodes before and after discharging, respectively. Inset figure in Fig. 8(b) shows the SAED pattern of the black particle.

nice capacity retention was achieved with no consumption of carbon by using nanoporous gold electrode [31]. Although the detail mechanism of Li_2CO_3 formation in the PP13TFSA based system is not clear yet, it is easily speculated that as in the previous papers [16,17], the Li_2CO_3 formation will gradually affect cycle performances such as coulomb efficiency and cycleability because of its highly positive equilibrium potential. Further investigation to prevent lithium peroxide from carbonation will be needed.

3.4. Cathode reaction mechanism

Based on our analytical results, cathode reaction mechanisms of the PP13TFSA and PC based Li–O_2 batteries were summarized in Fig. 10. Fig. 10 shows the cathode reaction route map of non-aqueous Li–O_2 batteries for mechanistic understanding. Route (i) is the originally expected reaction route on a cathode. Route (ii) denotes the conventional cathode reaction route including the PC based system. The last route (iii) represents the newly revised route including the PP13TFSA based system. At first, the two electron reduction process of O_2 gas on the cathode was drawn as in the expected reaction route (i). However, according to our previous papers [15,23,24] and many published papers [13,14,16–22], O_2 radical species (O_2^- and LiO_2) as intermediates were dominant in the non-aqueous media and then strongly influenced the following cathode reaction processes. Most of organic solvents typified by propylene carbonate (PC) were electrochemically and chemically vulnerable for the radical species. Therefore, as in the conventional route (ii), the decomposition of electrolyte solvent occurred and the decomposed species such as lithium alkylcarbonate were precipitated on a discharged cathode, resulting in CO_2 generation after recharging. On the other hand, the proposed solvents including PP13TFSA ionic liquid were highly stable against the radical species. Katayama et al. have also reported that some TFSA anion based ionic liquids had a high reversibility against oxygen reduction [32]. As a consequence, the solvation of radical species prevented the electrolyte solvents from being decomposed, and then converted the conventional reaction route (ii) into the revised one (iii). Li_2O_2 was mainly deposited as a discharge product and no chemical species due to electrolyte decomposition was generated, and thus, not CO_2 gas but O_2 gas evolved during recharging. A minor route to form Li_2CO_3 on the discharged cathode still remained and must be eliminated in the future. Above all, the stabilization of O_2 radical species was an important key to suppress the electrolyte decomposition and then to decide the discharge reaction process and the subsequent charging process on a cathode. It was, thus, concluded that our proposed PP13TFSA ionic liquid was a key component to satisfy the desirable cathode reaction, that is, Li_2O_2 formation.

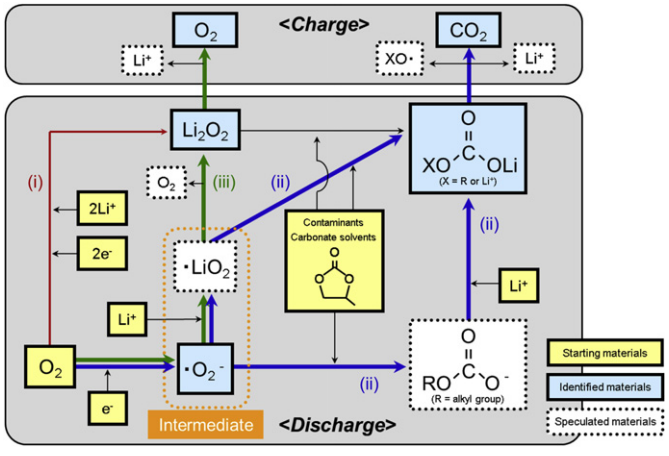

Fig. 10. Cathode reaction route map of non-aqueous Li–O_2 batteries for mechanistic understanding. Route (i) as in red line is the originally expected reaction route on a cathode. Route (ii) in blue line denotes the conventional cathode reaction route including the PC based system. The last route (iii) in green line represents the newly revised route including the PP13TFSA based system.

4. Conclusions

Using highly oxygen radical stable electrolyte solvent (PP13TFSA), the discharge–charge performances of the Li–O_2 batteries were confirmed, and then its cathode reaction mechanism was discussed in comparison with that of the conventional electrolyte solvent (PC). PP13TFSA based cell exhibited a great discharge–charge curve with low charging voltage (of around 3.3 V) and small voltage gap (of about 0.75 V), although the rate capability had to be further improved. Current performances indicated that mass transfer steps of Li^+ and O_2 in a cathode was a key parameter to establish much nicer rechargeable system. Based on several analytical techniques, a main discharge product and unwanted by-products were identified. In the PP13TFSA based Li–O_2 cell system, Li_2O_2 was deposited as a main discharge product and no decomposed species due to electrolyte decomposition were detected, whereas Li_2CO_3 as a minor by-product was still formed. Further investigation to eliminate a side reaction such as Li_2CO_3 formation will be continuously addressed. In summary, most of the cathode reaction was successfully improved by applying the highly oxygen radical stable electrolyte solvent (i.e. Li_2O_2 formation and O_2 generation). Electrolyte is still a key material to realize the promising Li–O_2 battery and must be updated for the future. Most of the systems including ours will have a mass transfer limiting step, overshadowing excellent potentials of rechargeable Li–O_2 batteries. Further material design such as catalyst, carbon [29] and electrolyte [33,34] to break through the limiting step will be intensively implemented.

References

[1] K.M. Abraham, Z. Jiang, J. Electrochem. Soc. 143 (1996) 1–5.
[2] J. Read, J. Electrochem. Soc. 149 (2002) A1190–A1195.
[3] T. Kuboki, T. Okuyama, T. Ohsaki, T. Takami, J. Power Sources 146 (2005) 766–769.
[4] T. Ogasawara, A. Debart, M. Holzapfel, P. Novak, P.G. Bruce, J. Am. Chem. Soc. 128 (2006) 1390–1393.
[5] S.J. Visco, E. Nimon, 12th International Meeting on Lithium Batteries, Abstr. 53, 2004.
[6] T. Zhang, N. Imanishi, Y. Shimonishi, A. Hirano, Y. Takeda, O. Yamamoto, N. Sammes, Chem. Commun. 46 (2010) 1661–1663.
[7] W. Xu, J. Xiao, J. Zhang, D. Wang, J.-G. Zhang, J. Electrochem. Soc. 156 (2009) A773–A779.
[8] C.O. Laoire, S. Mukerjee, E.J. Plichta, M.A. Hendrickson, K.M. Abraham, J. Electrochem. Soc. 158 (2011) A302–A308.
[9] Y.-C. Lu, H.A. Gasteiger, Y. Shao-Horn, J. Am. Chem. Soc. 133 (2011) 19048–19051.
[10] M. Hayashi, H. Minowa, M. Takahashi, T. Shodai, Electrochemistry 78 (2010) 325–328.
[11] P. Albertus, G. Girishkumar, B. McCloskey, R.S. Sanchez-Carrera, B. Kozinsky, J. Christensen, A.C. Luntz, J. Electrochem. Soc. 158 (2011) A343–A351.
[12] V.S. Bryantsev, M. Blanco, J. Phys. Chem. Lett. 2 (2011) 379–383.
[13] C.O. Laoire, S. Mukerjee, K.M. Abraham, E.J. Plichta, M.A. Hendrickson, J. Phys. Chem. 113 (2009) 20127–20134.
[14] Y.-C. Lu, H.A. Gasteiger, E. Crumlin, R. McGuire Jr., Y. Shao-Horn, J. Electrochem. Soc. 157 (2010) A1016–A1025.
[15] F. Mizuno, S. Nakanishi, Y. Kotani, S. Yokoishi, H. Iba, Electrochemistry 78 (2010) 403–405.
[16] S.A. Freunberger, Y. Chen, Z. Peng, J.M. Griffin, L.J. Harwick, F. Barde, P. Novak, P.G. Bruce, J. Am. Chem. Soc. 133 (2011) 8040–8047.
[17] S.A. Freunberger, Y. Chen, N.E. Drewett, L.J. Hardwick, F. Barde, P.G. Bruce, Angew. Chem. Int. Ed. 50 (2011) 8609–8613.
[18] B.D. McCloskey, D.S. Bethune, R.M. Shelby, G. Girishkumar, A.C. Luntz, J. Phys. Chem. Lett. 2 (2011) 1161–1166.

[19] B.D. McCloskey, R. Scheffler, A. Speidel, D.S. Bethune, R.M. Shelby, A.C. Luntz, J. Am. Chem. Soc. 133 (2011) 18038–18041.
[20] J. Xiao, J. Hu, D. Wang, D. Hu, W. Xu, G.L. Graff, Z. Nie, J. Liu, J.-G. Zhang, J. Power Sources 196 (2011) 5674–5678.
[21] Y.-C. Lu, D.G. Kwabi, K.P.C. Yao, J.R. Harding, J. Zhou, L. Zuin, Y. Shao-Horn, Energy Environ. Sci. 4 (2011) 2999–3007.
[22] R. Black, S.H. Oh, J.-H. Lee, T. Yim, B. Adams, L.F. Nazar, J. Am. Chem. Soc. 134 (2012) 2902–2905.
[23] F. Mizuno, S. Nakanishi, A. Shirasawa, K. Takechi, T. Shiga, H. Nishikoori, H. Iba, Electrochemistry 79 (2011) 876–881.
[24] K. Takechi, S. Higashi, F. Mizuno, H. Nishikoori, H. Iba, T. Shiga, ECS Electrochem. Lett. 1 (2012) A27–A29.
[25] B.D. McCloskey, A. Speidel, R. Scheffler, D.C. Miller, J.S. Hummelsheoj, J.K. Norskov, A.C. Luntz, J. Phys. Chem. Lett. 3 (2012) 997–1001.
[26] H. Sakaebe, H. Matsumoto, Electrochem. Commun. 5 (2003) 594–598.
[27] S. Nakanishi, F. Mizuno, K. Nobuhara, T. Abe, H. Iba, Carbon 50 (2012) 4794–4803.
[28] S. Nakanishi, F. Mizuno, T. Abe, H. Iba, Electrochemistry 80 (2012) 783–786.
[29] K. Minami, M. Imano, F. Mizuno, H. Nishikoori, H. Iba, 16th International Meeting on Lithium Batteries, Abstr. P2-323, 2012.
[30] M. Keskes, Z. Reeve, N. Drewett, L. Hardwick, P.G. Bruce, G.R. Goward, C.P. Grey, 16th International Meeting on Lithium Batteries, Abstr. P2-282, 2012.
[31] Z. Peng, S.A. Freunberger, Y. Chen, P.G. Bruce, Science (2012). http://dx.doi.org/10.1126/science.1223985.
[32] Y. Katayama, H. Onodera, M. Yamagata, T. Miura, J. Electrochem. Soc. 151 (2004) A59–A63.
[33] H. Nakamoto, Y. Suzuki, F. Mizuno, H. Nishikoori, K. Takechi, S. Higashi, T. Asaoka, H. Iba, 16th International Meeting on Lithium Batteries, Abstr. P2-326, 2012.
[34] K. Takechi, S. Higashi, H. Nakamoto, F. Mizuno, H. Nishikoori, H. Iba, T. Asaoka, 16th International Meeting on Lithium Batteries, Abstr. P2-344, 2012.